Supporting Information

Amorphous ReS_2 Decorated TiO_2 Nanowire Arrays for Highly Efficient Nitrogen Reduction

Xiaoying Lu, Hua Li, Yantao Wang, Junfeng Huang, Cailing Xu*

State Key Laboratory of Applied Organic Chemistry, Laboratory of Special Function Materials and Structure Design of the Ministry of Education, College of Chemistry and Chemical Engineering, Lanzhou University, Lanzhou 730000, China

*****Email: xucl@lzu.edu.cn

1. Experimental section

1.1 Materials

All materials were directly used without further purification. Ti plate (99.9% purity, 5 mm thickness) and ammonium perrhenate (NH_4ReO_4) were purchased from Alfa Aesar. Thioacetamide (TAA), salicylic acid ($C_7H_6O_3$), sodium citrate dehydrate ($C_6H_5Na_3O_7•2H_2O$), hydrochloric acid (HCl), anhydrous ethanol, acetone, hydrazine hydrate ($N_2H_4•H_2O$) and sodium hypochlorite (NaClO) were obtained from Cologne Sinopharm Chemical Reagent Co., Ltd. (China). Sodium nitroferricyanide (Ⅲ) dihydrate ($C_5FeN_6Na_2O$), sodium hydrate (NaOH) and sulfuric acid (H_2SO_4) were bought from Damao Chemical Reagent Factory (Tianjin, China). Ammonium chloride (NH_4Cl) and anhydrous sodium sulfate (Na_2SO_4) were purchased from Aladdin Ltd. (Shanghai, China). Electrolyte solutions were prepared with by Deionized water (DI, Millipore, 18.2 MΩ cm).

1.2 Preparation of samples

1.2.1 Synthesis of TiO_2 nanowires

The detail preparation process was similar to that reported in our previous report[1]. Firstly, Ti plates (1.0 cm × 2.0 cm) were sonicated with CH_3COCH_3, C_2H_5OH and H_2O for 20 min, respectively. Secondly, the cleaned Ti foil was put into a 25 mL Teflon-lined autoclave filled with 10 mL of 2.5 % HCl aqueous solution and kept at 190 ºC for 12 h. After being cooled to room temperature, the Ti foil was completely washed with deionized water several times and dried in the air. Finally, the as-prepared Ti nanowires (NWs) were then annealed at 450 ºC for 10 h to form TiO_2 NWs.

1.2.2 Synthesis of ReS_2/TiO_2 heterostructure

ReS_2 nanosheets were grafted on the surface of TiO_2 NWs via a facile hydrothermal process. 40 mg of NH_4ReO_4 (3 mM) and 60 mg of TAA were dissolved in 30 mL of deionized water and stirred for 30 min to obtain a mixed solution. Then, TiO_2 NWs soaked in the mixed solution in a 50 mL Teflon-lined stainless steel autoclave and kept at 200 ºC for 24 h. After being cooled naturally to room temperature, the TiO_2 NWs was taken out, washed with deionized water and anhydrous ethanol, and dried at 60 ^oC overnight. By adjusting the amount of the precursor NH_4ReO_4, the attained samples were named as: ReS_2/TiO_2-0.75 (0.75 mM), ReS_2/TiO_2-1 (1.0 mM) and ReS_2/TiO_2-1.5 (1.5 mM), respectively.

1.3 Catalyst Characterizations

The preparedTiO_2 NWs and ReS_2/TiO_2 heterostructures was determined by X-ray diffraction (XRD) using a Rigaku D/M ax-2400 diffractometer operated at 40 kV and

40 mA with Cu Kα radiation (λ = 0.15418 nm). Raman spectra measurements were carried out on a Raman spectrometer (Jobin Yvon Co., France) model HR800 and 532 nm laser as the excitation wavelength. Morphological properties of the TiO_2 NWs and ReS_2/TiO_2 heterostructures were examined by a field emission scanning electron microscopy (FESEM, JEOLJSM-S4800) operated at an accelerating voltage of 10.0 kV. The microstructure was determined by transmission electron microscopy (TEM, Tecnai^{TM} G2 F30). X-ray photoelectron spectroscopy (XPS) measurements were performed on a PHI-5702 instrument operated with a Mg-Kα excitation source (1253.6 eV). Binding energies (BE) were determined using the C 1s peak at 284.8 eV as a charge reference. Electron paramagnetic resonance (ESR) spectroscopy was obtained on a Bruker 200 spectrometer. The absorbance data of spectrophotometer were measured on U-3900H UV-vis spectrophotometer (Hitachi, Japan).

1.4 Electrochemical measurements

Electrochemical measurements were carried out on Metrohm Autolab workstation (PGSTAT302N, Metrohm) using a stand three-electrode configuration and gastight H-type electrolytic cell. In cathodic chamber, the as-prepared materials (an effective geometric area of 1.0×1.0 cm^2) and Ag/AgCl electrode (in saturated KCl electrolyte) were served as the working electrode and reference electrode, respectively. A graphite rod was used as counter electrode in the anodic chamber. The H type electrolytic cell was separated by a Nafion 211 membrane (Dupont) which was protonated by boiling in the 5% H_2O_2 aqueous and heating 0.5 M H_2SO_4 for 1 h, respectively, and then washing with ultrapure water for 6 h. All potentials measured were converted to the

reversible hydrogen electrode (RHE) through calibration with the following equation: E (V vs. RHE) = E (V vs. Ag/AgCl) + 0.197 + 0.059×pH (Number this equation).

Before electrolysis, the working electrode was immersed in the electrolyte for 2h to remove the influence of pollutants and N_2 and Ar was purged into the electrolyte for at least 30 min with a flowing rate of 50 mL min^{-1} to remove the air. Before feeding the gas into the electrolyte, it was further purified through 0.01 M H_2SO_4 and distilled water to remove the possible NH_3 and NO_x [2]. During electrolysis, high-purity N_2 was continuously fed into the cathodic compartment with a flow of 20 sccm. After NRR, the produced tail gas (e.g., N_2) was further absorbed by two-series tail gas absorbers (each absorber contains 50 mL of 0.01 M H_2SO_4 solution) to prevent the produced NH_3 during NRR with N_2 flow into air. Linear sweep voltammogram (LSV) was scanned at a rate of 5 mV s^{-1}. Chronoamperometry technology was applied to study the NH_3 synthesis performance.

The electrochemical impedance spectroscopy (EIS) of the electrodes were measured at -0.1 V versus RHE in the frequency range from 100 kHz to 0.01 Hz with an amplitude of 10 mV. To determine the double-layer capacitance (C_{dl}), a series of CV measurements were carried out at different scan rates (20, 40, 60, 80 and 100 mV•s^{-1}) in a non-Faradaic region (1.04-1.14 V vs. RHE).

1.5 Determination of Ammonia

The concentration of produced ammonia was detected by a reported indophenol blue method [3].

a) Stock reagent:

1) Chromogenic reagent (A): 1 M NaOH solution containing 5% sodium citrate and 5% sodium salicylate was prepared.

2) Oxidizing solution (B): 0.05 M NaClO solution (available chlorine 10-15%) was prepared.

3) Catalysing reagent (C): 1 wt % $C_5FeN_6Na_2O$ solution was prepared.

b) Standard solutions preparation

1) 1000 μg_{NH3}/mL solution: 0.3809 g of pre-dried NH_4Cl (105 ℃ for 4 h) was added in 100 mL of 0.1 M Na_2SO_4 solution.

2) 10 μg_{NH3}/mL solution: 1 mL of 1000 μg_{NH3}/mL stock solution was added in a 100 mL volumetric flask, and added 0.1 M Na_2SO_4 solution to the scale mark.

3) 0.2, 0.4, 0.8, 1.2, 1.6 and 2 mL of 10 μg_{NH3} mL^{-1} stock solution were separately added into a 20 mL volumetric flask and added 0.10 M Na_2SO_4 solution to the scale mark to obtain 0.1, 0.2, 0.4, 0.6, 0.8 and 1 μg_{NH3} mL^{-1} standard solutions.

c) UV-vis measurement

Typically, 2 mL of standard solutions or sample solution was firstly added to 10 mL of colorimetric tube, where 2 mL of regent (A), 1 mL of regent (B) and 0.2 mL of reagent (C) were then subsequently added. The mixed solution was kept at room temperature for 2 h and subjected to the UV-vis tests. The ammonia concentration was determined depending on the absorbance at a wavelength of 655 nm. The calibrated concentration-absorbance curve was provided in Fig. S5, which was y = 0.556x + 0.0576 (R^2=0.999). The ammonia yield rate was calculated based on the equation:

$$NH_3\ yield\ rate = \frac{c \times V}{A \times t} \qquad \text{(S1)}$$

Where c is the measured NH_3 concentration; V is the volume of the electrolyte; t is the electrolysis time, and A is the working electrode area (1.0×1.0 cm^2).

The Faradaic efficiency was calculated according to the following equation:

$$FE(\%) = \frac{3 \times F \times c \times V}{17 \times Q} \times 100\% \qquad \text{(S2)}$$

Where F is the Faraday constant (96485 C mol^{-1}), c is the measured NH_3 concentration, V is the volume of the electrolyte and Q is the total charge used for the electrodes (C).

1.6 Hydrazine quantification

The by-product of hydrazine was assessed by the method of Watt and Chrisp[4]. Typically, a mixture of pdimethylaminobenzaldehyde (5.99 g), concentrated HCl (30 mL) and C_2H_5OH (300 mL) were used as a color regent. In detail, 5.0 mL electrolyte pipetted from the cathodic chamber added into 5.0 mL of the above prepared color reagent. After standing the mixture solution at room temperature for 10 min, UV-vis absorption spectra was measured at a wavelength of 457 nm. The concentration (N_2H_4•H_2O)-absorbance curve was calibrated using standard hydrazine solution with a series of N_2H_4•H_2O concentrations (0, 0.2, 0.6, 1.2, 1.5, 2.0 μg mL^{-1}). The fitting curve (y=0.162x+0.04, R^2=0.998) shows good linear relation between the absorbance value and hydrazine concentration.

2. Supplementary Figures

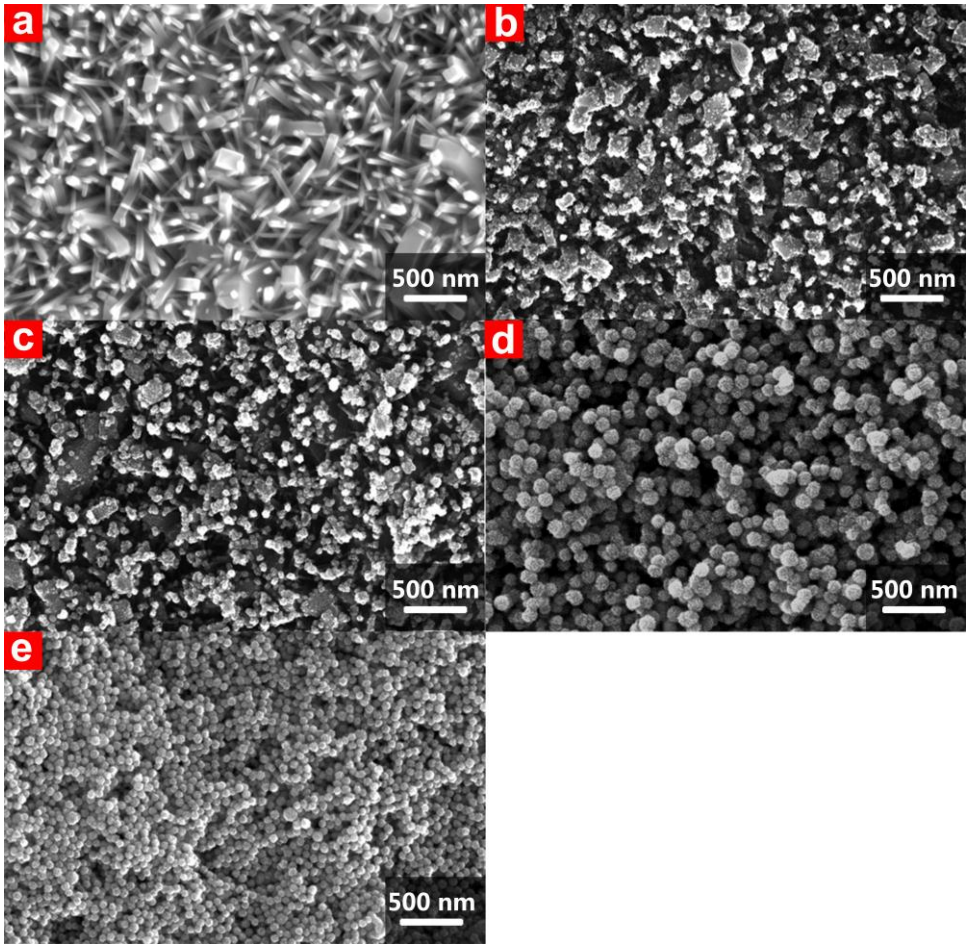

Fig. S1 SEM images of (a) TiO_2 NWs, (b) ReS_2/TiO_2-0.75, (c) ReS_2/TiO_2-1, (d) ReS_2/TiO_2-1.5 and (e) ReS_2/TiO_2-3 heterostructure.

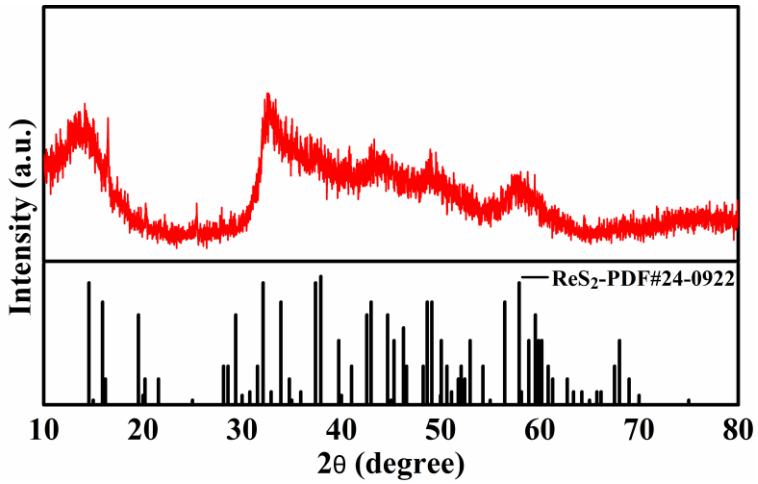

Fig. S2 XRD pattern of rhenium disulfide powders.

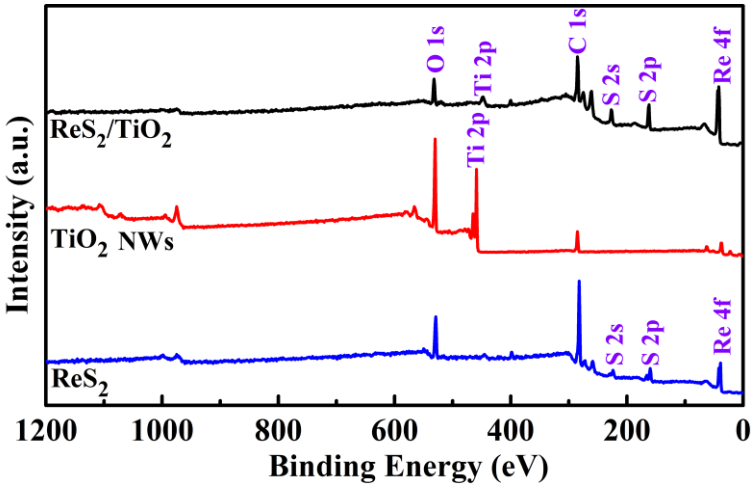

Fig. S3 Wide-scan survey XPS spectrum of ReS_2 powder, TiO_2 NWs and ReS_2/TiO_2 heterostructure.

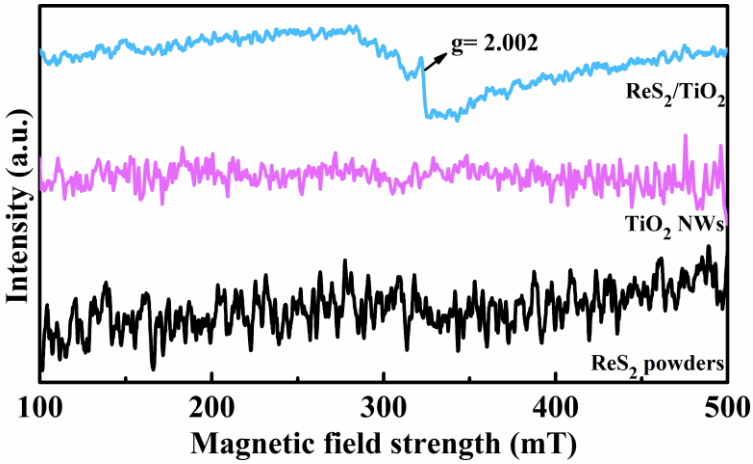

Fig. S4 EPR spectra of ReS_2/TiO_2 heterostructure, TiO_2 NWs and ReS_2 powders.

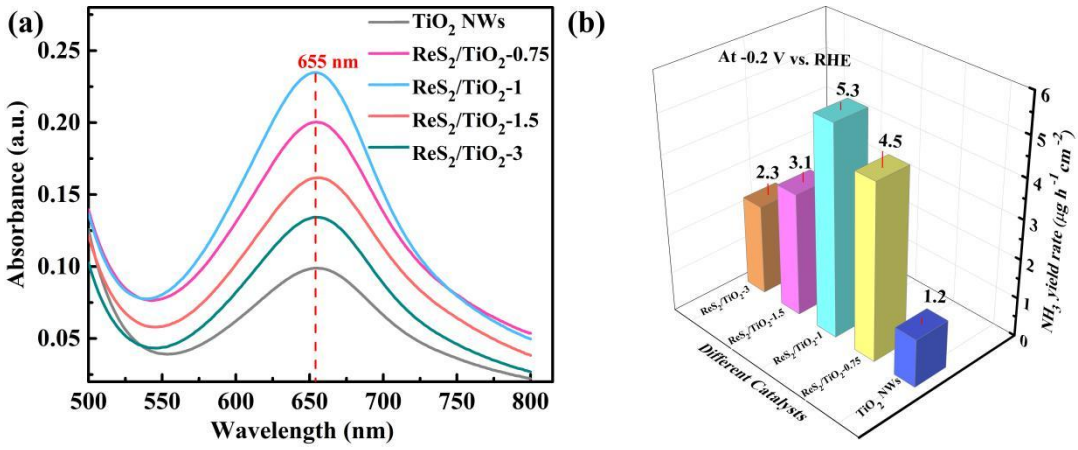

Fig. S5 (a) UV-vis absorbance and (b) NH_3 yield rate of TiO_2 NWs, ReS_2/TiO_2-0.75, ReS_2/TiO_2-1, ReS_2/TiO_2-1.5 and ReS_2/TiO_2-3 at -0.2 V vs. RHE.

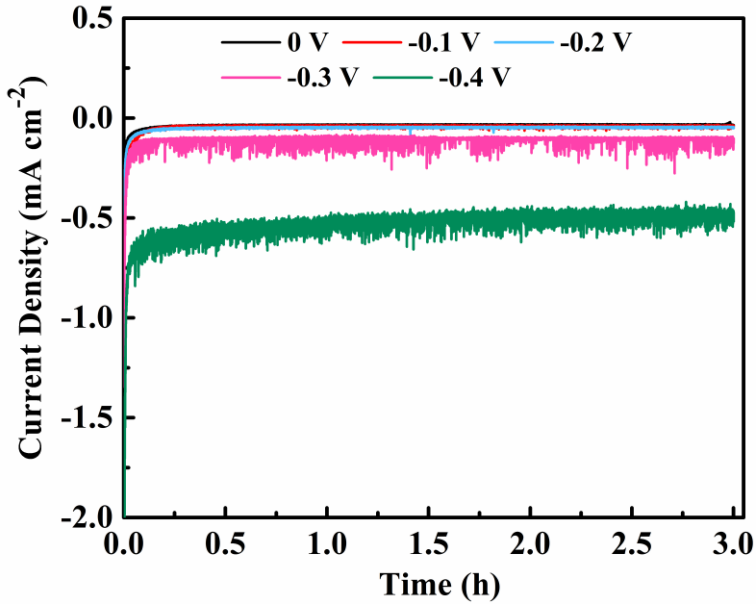

Fig. S6 Chronoamperometry curves of ReS_2/TiO_2 heterostructure at different potentials for 3 h in N_2-saturated 0.1 M Na_2SO_4 electrolytes.

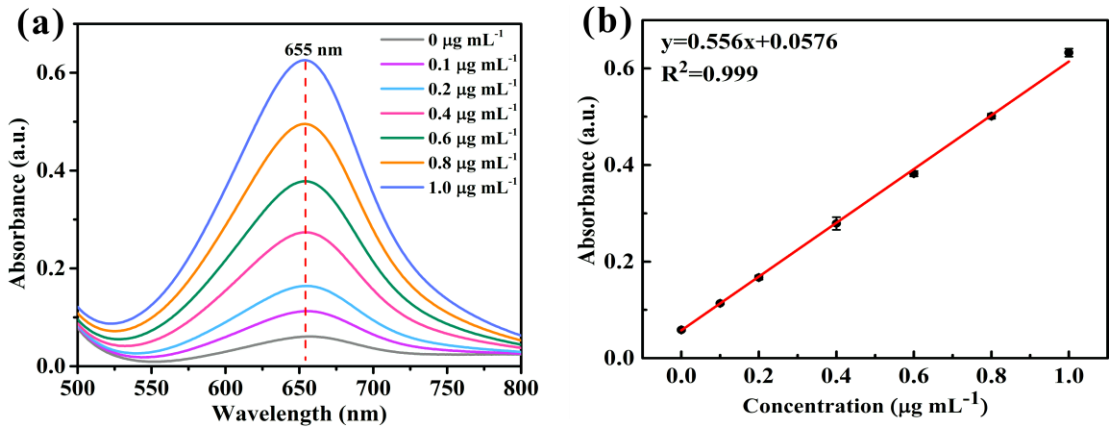

Fig. S7 Standard curves for NH_4Cl solution with different concentrations in 0.1 M Na_2SO_4 by indophenol blue colorimetric method. (a) UV-vis spectra of various ammonia concentrations after stained with indophenol indicator for 2 h and (b) the corresponding linear fitting between absorbance and NH_4Cl concentration.

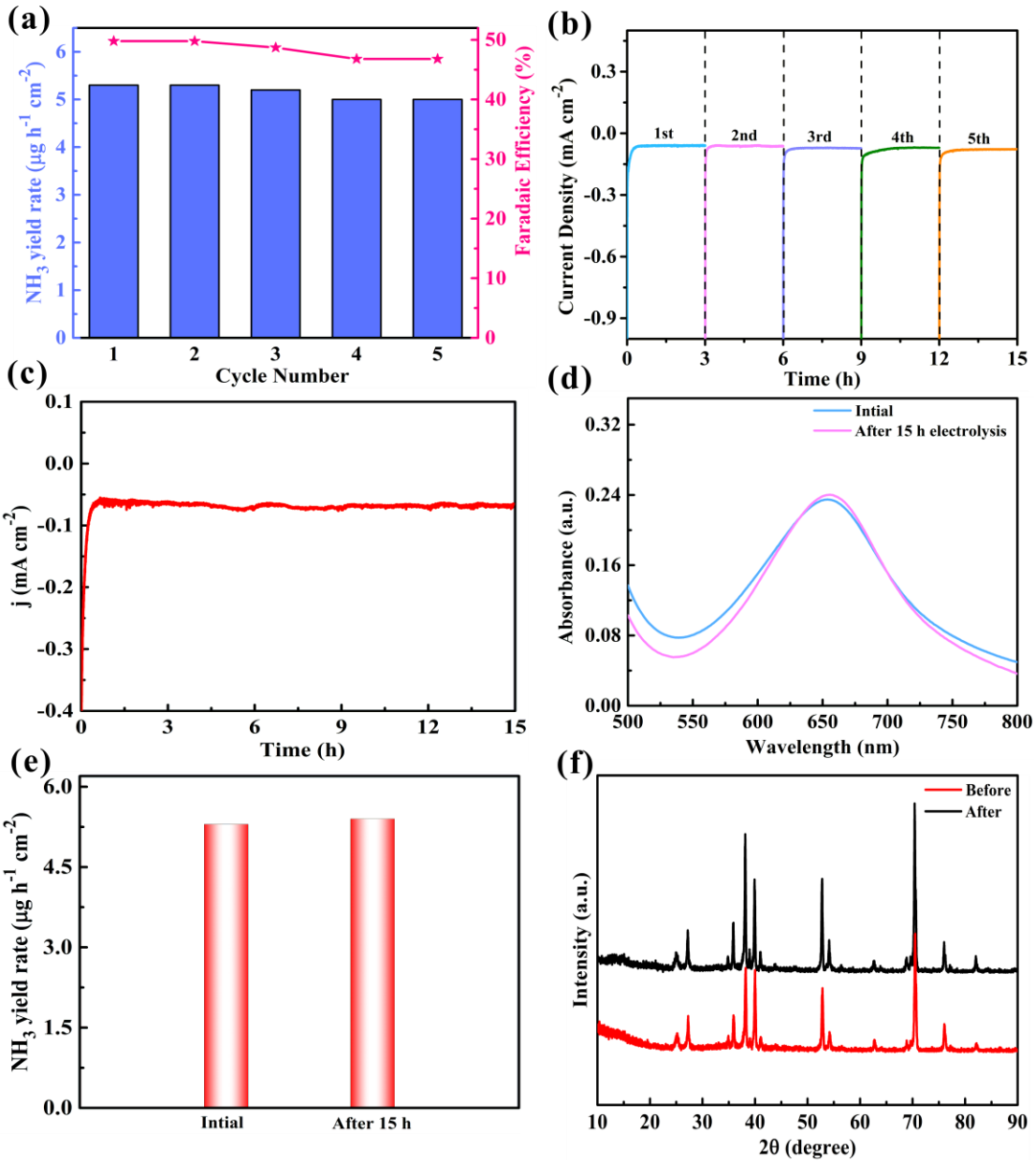

Fig. S8 (a) The NH_3 yield rate and FE over five successive measurements, (b) Chronoamperometry curves of ReS_2/TiO_2 heterostructure reuse five times, (c) Chronoamperometry curve at -0.2 V vs. RHE working continuously for 15 h, (d) UV-vis absorption spectra of solutions before and after the long-term chronoamperometric measurement, (e) NH_3 yield rate at -0.2 V vs. RHE after electrolysis for 3 h before and after long-term electrolysis and (f) XRD patterns of ReS_2/TiO_2 heterostructure before and after recycling test.

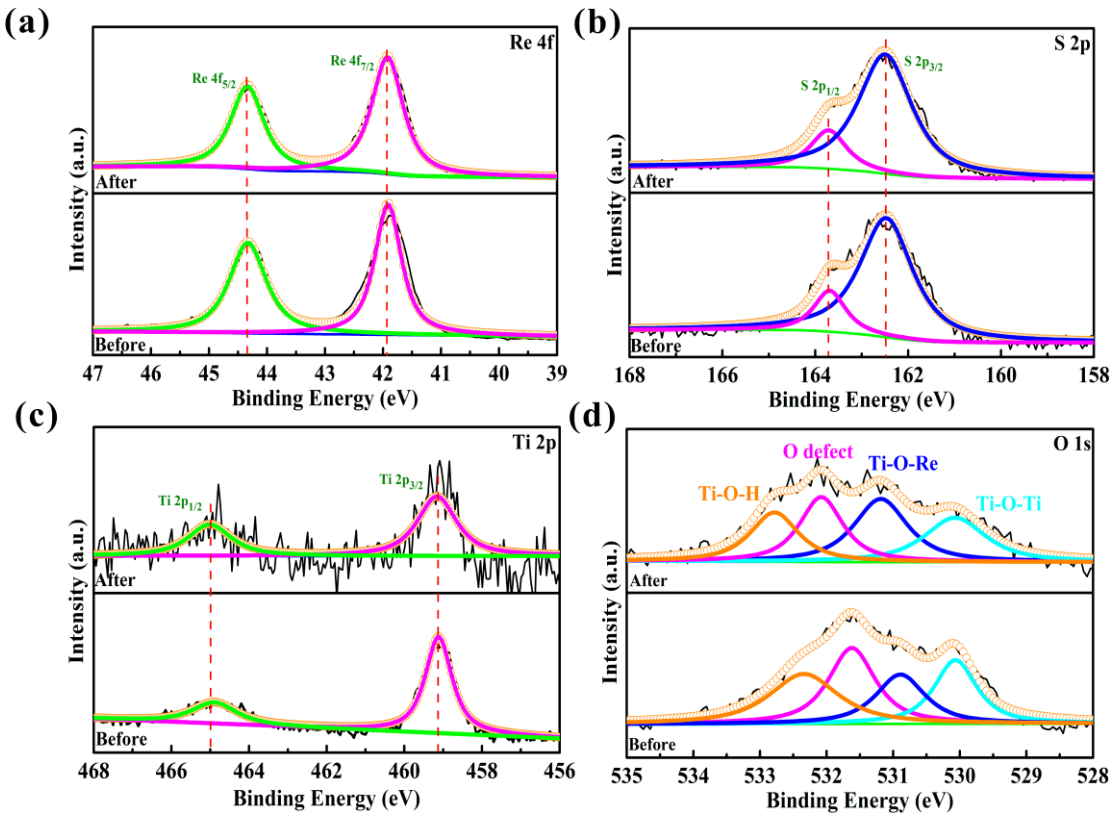

Fig. S9 High resolution XPS spectrum for ReS_2/TiO_2 heterostructure before and after recycling test: (a) Re 4f, (b) S 2p, (c) Ti 2p and (d) O 1s.

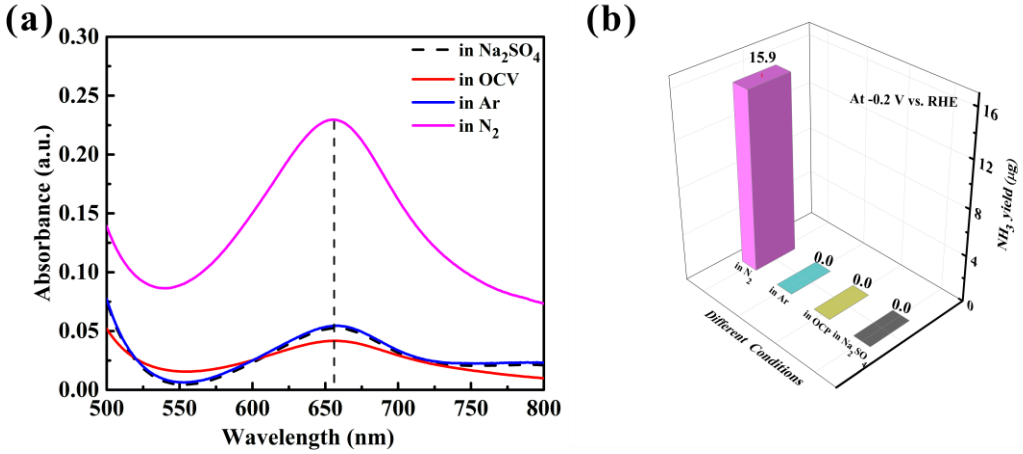

Fig. S10 (a) UV-vis absorption spectra of the electrolytes stained with indophenol indicator after 3 h potentiostatic electrolysis on ReS_2/TiO_2 heterostructure in different conditions and (b) the corresponding of NH_3 yield.

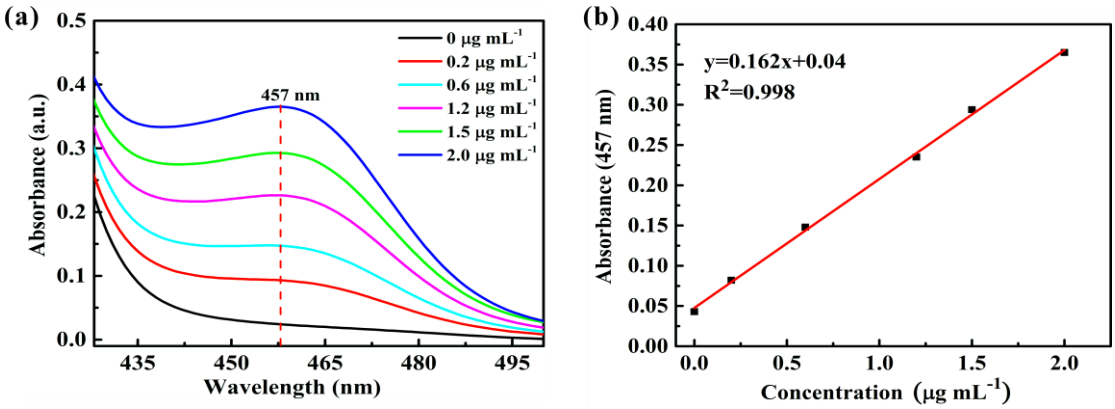

Fig. S11 Standard curves for hydrazine with different concentrations in 0.1 M Na_2SO_4 by the Watt and Chrisp method. (a) UV-vis spectra and (b) corresponding linear fitting between absorbance at 457 nm and hydrazine concentration.

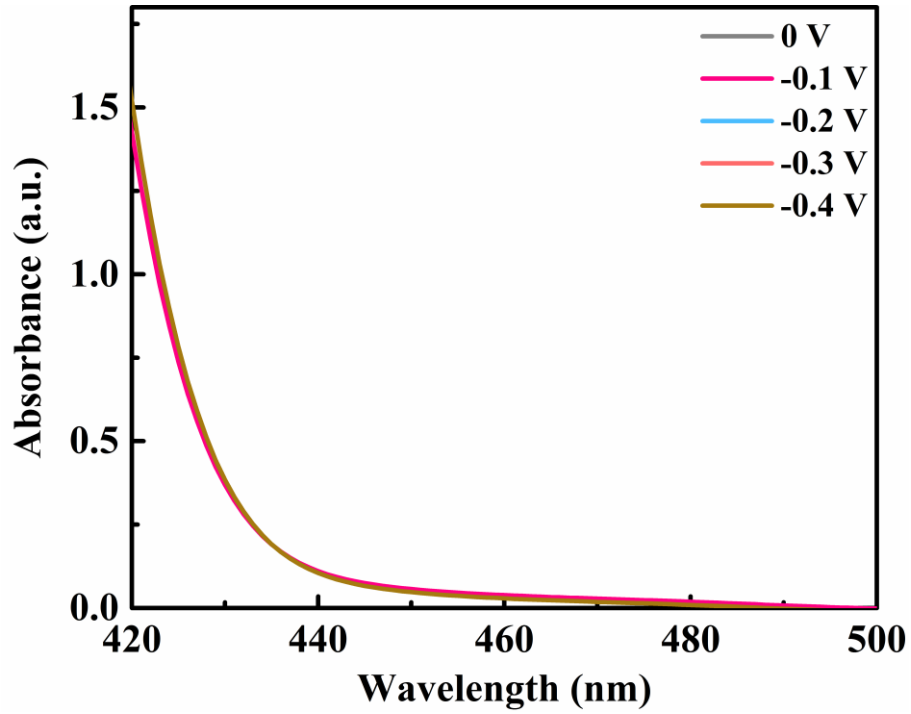

Fig. S12 Typical UV-vis spectra for detecting hydrazine in the cathodic chamber after electrolysis at different potentials in 0.1 M Na_2SO_4.

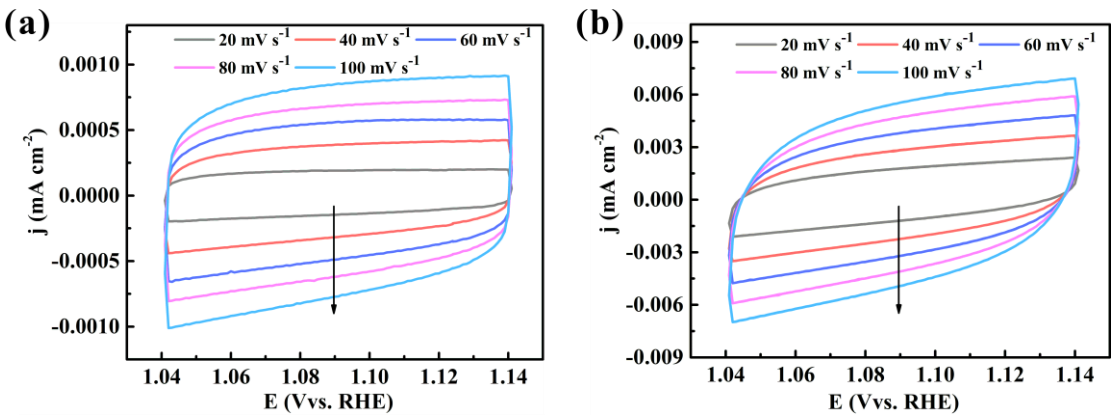

Fig. S13 Electrochemical cyclic voltammetry curves at different potential scanning rates for (a) TiO_2 NWs and (b) ReS_2/TiO_2 heterostructure.

Table S1. Comparison of the NRR activity of ReS_2/TiO_2 electrocatalyst with other aqueous-based catalysts reported recently under ambient conditions.

Catalysts	Electrolytes	NH_3 production rate	Faradaic efficiency	Reference
Mxene	0.5 M Li_2SO_4	4.70 μg h^{-1} cm^{-2}	5. 8 %	5
TiO_2/Ti	0.1 M Na_2SO_4	5.60 μg h^{-1} cm^{-2}	2.5 %	6
MoS_2/CC	0.1 M Na_2SO_4	4.9 μg h^{-1} cm^{-2}	1.2 %	7
SnS_2@Ni	0.1 M Na_2SO_4	9.1710^{-10} mol s^{-1} cm^{-2}	10.8 %	8
Bi-CeO_2	0.5 M K_2SO_4	6.3 μg h^{-1} cm^{-2}	8.6 %	9
Au nanorod	0.1 M KOH	1.6 μg h^{-1} cm^{-2}	4 %	10
CrN	0.05 M H_2SO_4	12.9 μg h^{-1} $mg^{-1}_{cat.}$	15.1 %	11
TiO_2-rGO	0.1 M Na_2SO_4	15.1 μg h^{-1} $mg^{-1}_{cat.}$	3.3 %	12
Y-TiO_2-C	0.1 M HCl	6.3 μg h^{-1} mg^{-1}	11.0 %	13
Ru-TiO_2-Vo	0.1 M KOH	2.10 μg h^{-1} cm^{-2}	0.8 %	14
SnO_2	0.1 M Na_2SO_4	9.0 μg h^{-1} cm^{-2}	2.2 %	15
DG-800	0.01 M H_2SO_4	4.3 μg h^{-1} $mg^{-1}_{cat.}$	8.5 %	16
S_v-Sb_2S_3	0.1 M Na_2SO_4	10.8 μg h^{-1} $mg^{-1}_{cat.}$	3.8 %	17
Ag nanosheet	0.1 M HCl	2.8 μg h^{-1} cm^{-2}	4.8 %	18
P-doped LDHs	0.1 M Na_2SO_4	1.72×10^{-10} mol s^{-1} cm^{-2}	23 %	19
$Pd_{0.2}Cu_{0.8}$/rGO	0.1 M KOH	2.8 μg h^{-1} $mg^{-1}_{cat.}$	-	20
ReS_2/TiO_2	0.1 M Na_2SO_4	5.3 μg h^{-1} cm^{-2}	6.7 %	This work

Reference:

1 C. Xu, H. Geng, R. Bennett, D. A. Clayton, S. Pan, *J. Phys. Chem. C,* 2013, *117*, 1849-1856.

2 F. Zhou, L. M. Azofra, M. Ali, M. Kar, A. N. Simonov, C. McDonnell-Worth, C. Sun, X. Zhang, D. R. MacFarlane, *Energy Environ. Sci.*, 2017, *10*, 2516-2520.

3 D. Zhu, L. Zhang, R. E. Ruther, R. J. Hamers, *Nature Mater.*, 2013, *12*, 836-841.

4 G. W. Watt, J. D. Chrisp, *Anal. Chem.*, 1952, *24*, 2006-2008.

5 Y. Luo, G. F. Chen, L. Ding, X. Chen, L. X. Ding, H. Wang, *Joule*, 2019, *3*, 279-289.

6 R. Zhang, X. Ren, X. Shi, F. Xie, B. Zheng, X. Guo, X. Sun, *ACS Appl. Mater. Inter.*, 2018, *10*, 28251-28255.

7 L. Zhang, X. Ji, X. Ren, Y. Ma, X. Shi, Z. Tian, A. M. Asiri, L. Chen, B. Tang, X. Sun, *Adv. Mater.*, 2018, *30*, 1800191.

8 X. Chen, Y. T. Liu, C. Ma, J. Yu, B. Ding, *J. Mater. Chem. A*, 2019, **7,** 22235-22241.

9 Y. Liu, C. Li, L. Guan, K. Li, Y. Lin, *J. Phys. Chem. C*, 2020, 124, 18003-18009.

10 D. Bao, Q. Zhang, F. L. Meng, H. X. Zhong, M. M. Shi, Y. Zhang, J. M. Yan, Q. Jiang, X. B. Zhang, *Adv. Mater.*, 2017, 29, 1604799.

11 W. Guo, Z. Liang, Y. Tang, K. Cai, Q. Tianjie, Y. Wu, K. Zhang, S. Gao, R. Zou, *J. Mater. Chem. A*, 2021, DOI: 10.1039/D0TA11727G.

12 X. Zhang, Q. Liu, X. Shi, A. M. Asiri, Y. Luo, X. Sun, T. Li, *J. Mater. Chem. A*, 2018, *6*, 17303-17306.

13 L. Yang, C. Choi, S. Hong, Z. Liu, Z. Zhao, M. Yang, H. Shen, A. W. Robertson, H.

Zhang, T. W. B. Lo, Y. Jung, Z. Sun, *Chem. Commun.*, 2020, *56*, 10910-10913.

14 S. Cheng, Y. J. Gao, Y. L. Yan, X. Gao, S. H. Zhang, G. L. Zhuang, S. W. Deng, Z. Z. Wei, X. Zhong, J. G. Wang, *J. Energy Chem.*, 2019, *39*, 144-151.

15 L. Zhang, X. Ren, Y. Luo, X. Shi, A. M. Asiri, T. Li, X. Sun, *Chem. Commun.*, 2018, *54*, 12966-12969.

16 Y. Du, C. Jiang, W. Xia, L. Song, P. Li, B. Gao, C. Wu, L. Sheng, J. Ye, T. Wang, J. He, *J. Mater. Chem. A*, 2020, 8, 55-61.

17 X. Wang, J. Bai, Y. Wang, X. Lu, Z. Zou, J. Huang, C. Xu, *Green Energy & Environment*, 2020, DOI: https://doi.org/10.1016/j.gee.2020.11.016.

18 H. Huang, L. Xia, X. Shi, A. M. Asiri, X. Sun, *Chem. Commun.*, 2018, *54*, 11427-11430.

19 Y. T. Liu, L. Tang, J. Dai, J. Yu, B. Ding, *Angew. Chem. Int. Ed.*, 2020, *59*, 13623-13627.

20 M. M. Shi, D. Bao, S. J. Li, B. R. Wulan, J. M. Yan, Q. Jiang, *Adv. Energy Mater.*, 2018, 8, 1800124.